Outdoor Measurements Using an Optical Wireless Link for Fixed-Access Applications

Dominic Schulz, Julian Hohmann, Peter Hellwig, Jonas Hilt, Christian Schmidt, *Graduate Student Member, IEEE*, Ronald Freund, and Volker Jungnickel, *Member, IEEE*

(Invited Paper)

***Abstract*—In this paper, results are presented from a long-term outdoor field trial using a rate-adaptive, LED-based optical wireless link over 100 m rooftop-to-rooftop distance. The optical link is installed in parallel to a 60 GHz link, enabling a direct comparison of both technologies for the same conditions by logging signal-to-noise ratios, data rates, and weather conditions. A model for the optical link has been developed for performance prediction based on weather data. Besides studying particular weather events, an analysis was conducted for the whole statistics. Results indicate that availability of the optical link was higher than 99.99%, despite severe weather conditions due to fog, rain, and snow. Although both links offer several hundred megabit per second, the optical link has a higher data rate 99.8% of the time while the 60 GHz link has a more consistent performance. Correlation is weak in bad weather conditions, e.g., if the SNR is low for the 60 GHz link due to heavy rain, the SNR in the optical link is high as the fog is light at the same time. Further measurements verify low latencies in the millisecond to sub-millisecond range for the optical link. Results indicate that the optical link is a promising low-cost solution for fixed access applications such as the replacement of fiber on the last 100 m to the end user, also denoted as wireless-to-the-home, and as a backhaul for Wi-Fi and small mobile radio cells.**

***Index Terms*—Backhaul, fronthaul, LED, millimeter wave, optical wireless communication, small cell, wireless-to-the-home.**

I. Introduction

THE increasing demand for higher capacity of broadband services as well as new functionalities for the Internet of Things (IoT), such as ultra-reliable low latency communications (URLLC), drive the development of the next generation of fixed and mobile networks [1]. In order to meet the new key performance indicators (KPI), fixed access networks connecting enterprises, radio base stations and homes go beyond the capabilities of digital subscriber lines (DSL). In the mobile network, the expected increase of mobile data traffic per geographical area by a factor of 1000 and the 10 to 100 times higher user data rates [2] can no longer be served from the existing macro cell (MC) sites, i.e., the network will be densified [3].

Fiber-to-the-home (FTTH) deployments and a densification of MCs in mobile networks by adding a large number of small cells (SC), ideally connected by fiber, are considered as key enablers to deploy next generation networks [4], [5]. The Telecom Infrastructure Project (TIP) noted that network operators spend more than half of their capital expenditure (CAPEX) in the fixed access domain, i.e., on the last few hundred meters connecting each individual end user, and that most of these costs are for digging the fiber, which is time-consuming as well. Hence, to serve the expected KPIs, operators will need substantial investments into their fixed access infrastructure in a relatively short period of time [6]. For this reason, the availability of alternative fixed-wireless solutions is of interest as they circumvent digging the fiber. The fixed-wireless approach can reduce cost and speed up the deployment, which is important in an increasingly competitive network infrastructure market. Replacing fiber by a fixed wireless link can be achieved by solutions where new spectrum is utilized with wide-enough bandwidth. Interesting candidates are millimeter-wave (mm-wave) technologies going up to several hundred GHz, as well as optical solutions. With average distances well below 100 m between street luminaires and residential buildings, the use of wireless technologies becomes attractive for the last mile. Complexity and cost of deployment can be reduced by connecting only the street lamps or traffic lights to the fiber network and then applying wireless links for the last link to the end customer. Inspired by FTTH, this approach is called wireless-to-the-home (WTTH) and is discussed actively among network and service providers; initial pilot installations are deployed [7], [8]. Fiber replacement may be straightforward for less-demanding broadband applications. However, additional features, such as time and frequency synchronization, high availability and low latency are required for the new IoT and URLLC services and the deployment of small radio cells. Optical wireless (OW) technology offers an alternative to relief the radio spectrum and performance, matching the requirements of next generation of fixed and mobile networks.

With peak data rates up to 1 Gbps per end user and latency requirements in the range of multiple 10 ms, the requirements for

Manuscript received July 25, 2018; revised October 19, 2018; accepted October 19, 2018. Date of publication October 26, 2018; date of current version February 20, 2019. *(Corresponding author: Dominic Schulz.)*

D. Schulz, J. Hohmann, P. Hellwig, J. Hilt, R. Freund, and V. Jungnickel are with the Fraunhofer Heinrich Hertz Institute, Berlin 10587, Germany (e-mail: dominic.schulz@hhi.fraunhofer.de; julian.hohmann@hhi.fraunhofer.de; peter.hellwig@hhi.fraunhofer.de; jonas.hilt@hhi.fraunhofer.de; Ronald.Freund@hhi.fraunhofer.de; volker.jungnickel@hhi.fraunhofer.de).

C. Schmidt is with the Department of Photonic Networks and Systems-Fraunhofer Heinrich-Hertz-Institut, Berlin 10587, Germany (e-mail: christian.schmidt@hhi.fraunhofer.de).

Color versions of one or more of the figures in this paper are available online at http://ieeexplore.ieee.org.

Digital Object Identifier 10.1109/JLT.2018.2878362

WTTH are apparent. However, for integrating SCs for mobile radio, it is important to understand the radio network architecture and corresponding requirements for data rate, latency and reliability for both backhaul (BH) and fronthaul (FH).

SCs require tight coordination as the frequency of handovers is increased and interference scenarios are more complex. The centralized radio access network (C-RAN) architecture became popular in which remote radio heads (RRH) are connected via the common public radio interface (CPRI), denoted as FH, to a centralized baseband unit (BBU) [9], while the BBU connects to the mobile core network via the BH. Centralization can cut costs down to 50% [9], [10]. Moreover, higher flexibility and scalability are enabled. However, CPRI requires huge data rates besides low latency and negligible jitter, e.g., a 2×2 MIMO LTE SC with 20 MHz bandwidth requires 2.5 Gbps for the transport of I-Q data at high resolutions [11]. In 5G, CPRI is no longer feasible, considering higher bandwidth and significantly more antennas [12]. To offload data to SCs [13], new split points (SPs) between the BBU and the RRH have been defined [14], [15]. Requirements vary between 50 and 500 Mbps for data rates, between 250 μs and 2 ms for latencies and between 99% and 99.99% for availability depending on the SP. Since the demands are rather diverse, there is no sole mobile BH solution, making the analysis of alternatives evident.

The use of LED based optical wireless communication (OWC) for short-range indoor applications, also denoted as visible light communication or Li-Fi, has become popular in recent years. Originally meant for high-speed mobile access, functionalities like multi-user support and handover, similar to mobile radio have been demonstrated, offering a complementary approach to radio technologies like Wi-Fi or as a relief for the overcrowded radio frequencies (RF) in cooperative use [16], [17]. To achieve high efficiency, algorithms and methods from radio communication, like rate adaptation with orthogonal frequency division multiplexing (OFDM), are combined with low-cost optical frontends enabling high modulation bandwidths using standard high-power LEDs and silicon pin (Si-PIN) photodiodes (PD), resulting in multi-Gbps speed [18], [19]. The same low-cost approach is applicable for longer distances in outdoor point-to-point scenarios. OWC systems provide enough data rate as well as sophisticated signal processing enabling one-way latencies in the order of a few milliseconds. Moreover, RF bands, commonly used for mobile FH and BH, e.g., mm-wave, can be relieved by offloading data to the optical spectrum and reducing interference in dense installation scenarios.

Significant research has been carried out for OWC based on visible light LEDs and lasers in outdoor scenarios [20]–[22], with focus on turbulences [23] and several other fields like military and satellite applications [24], [25]. Available systems offer a wide range of performances starting from 10 Mbps of the open source approach RONJA [26] or the KORUZA [27] system with a rather free space optics design based on small form pluggable transceivers and mechanical tracking up to 1 Gbps.

The investigations presented in this paper are different and based on an OW system originally developed for mobile access [28]–[30]. Low cost optical components together with a wideband driver and a low noise transimpedance amplifier are chosen. Combined with DC-biased OFDM and rate adaptation, a peak data rate of 1 Gbps is reached. Due large-area PDs, no tracking is needed and alignment is simple due to the enlarged, homogenous illuminated spot and field-of-views (FOV).

The objective of this article is to conduct measurements in a real outdoor scenario and analyze the influence of weather effects. To compare the optical link with state-of-the-art radio links, a commercial 60 GHz mm-wave link is setup in parallel to evaluate link performances in various atmospheric conditions. This way we aim at answering the question, if OWC is able to meet the requirements concerning data rates, latencies and availabilities for next generation FH and BH as well as WTTH.

The paper is organized as follows. In Section II, a mathematical model for the OW link is presented which enables link performance prediction for different climatic conditions worldwide. Results are validated with measured values from the field trial. In Section III, the installation of both the OW and the 60 GHz link at the measurement site is described. Exemplary weather events are discussed in Section IV followed by statistical results. Moreover, correlation of performance between both links is analyzed and latency measured for different traffic loads. Section V concludes the paper and provides an outlook on future work.

II. Mathematical Model and Availability Estimation

In this section, the line-of-sight (LOS) probability expression for dense urban scenarios is provided and a mathematical model is introduced for the OW link. Signal-to-noise ratios (SNR) are computed and external weather data used to predict the link performance for different distances and climatic conditions.

A. Line-of-Sight Probability

Using OWC for the link to a SC or WTTH requires a free LOS between the SC or building and the aggregation point, e.g., the overlapping MC or street lamp. For BH this can become an issue especially in dense city scenarios, where high buildings yield to urban street canyons. Note that the LOS probability between the base station and the user device in an urban environment is well known in mobile communications for different scenarios [31]. In this subsection, theoretical LOS probability for dense urban scenarios is compared with measurements from the European Union project WINNER.

The most relevant scenario for the discussed applications, 3D-UMa considers a MC installed on one out of multiple high-rise building above the surrounding buildings, representing a metropolitan city center with very dense development. Depending on the actual building development, the LOS probability P_{UMa} is modeled as follows, assuming the height of the SC below 10 m

$$P_{UMa} = \begin{cases} 1, & d \leq 18 \text{ m}; \\ \frac{18}{d} + e^{\left(-\frac{d}{63}\right)} \cdot \left(1 - \left(\frac{18}{\text{d}}\right)\right), & 18 \text{ m} < d; \end{cases} \quad (1)$$

with d being the distance between the MC and the SC. Additionally results are available for LOS measurements within the WINNER project in an urban area of Berlin, indicating a LOS probability of 62% at 200 m [32]. In Fig. 1, the LOS probability from (1) is shown with respect to the distance and the

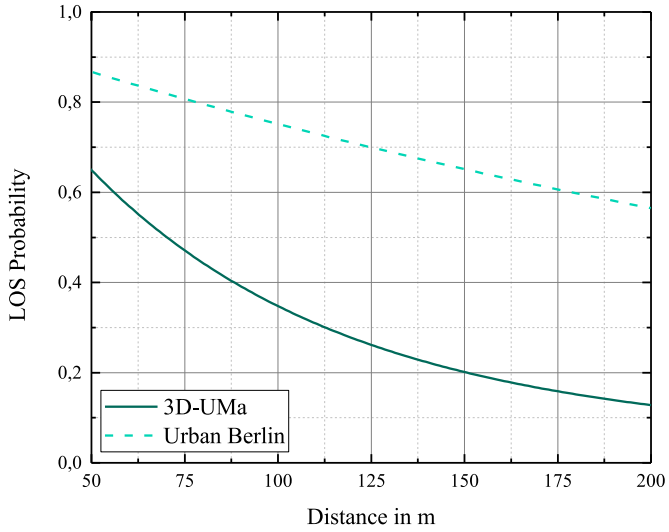

Fig. 1. LOS probability for a dense urban scenario with multiple high-rise buildings (3D-UMa) and measured LOS probabilities from the WINNER project (Urban Berlin).

results from the WINNER measurements. It can be seen that the calculated LOS probability is between 65% and 13% in the 3D-UMa case for distances between 50 and 200 m. The urban Berlin measurements indicate that the actual LOS probability can differ substantially from the aforementioned model, due to actual building development. Most cities are less developed and, hence, LOS probability is rather high.

B. Mathematical OW Link Model

In this subsection, the mathematical model for the OWC system, used for the outdoor measurements is presented. Fig. 2 shows the block diagram with unidirectional signal transmission and the losses due to terrestrial transmission. In the following, formulas are provided for the signal generation, all losses resulting from the outdoor channel and the signal reception in order to calculate the SNR. To validate the model, we compare exemplary calculations to real field measurements. External weather data used with the model enable prediction of the link performance in different scenarios and climatic conditions.

The current through the LED I_{LED} is composed of the direct current (DC) I_{DC} biasing the LED and the AC current I_{Sig} carrying the data signal.

$$I_{LED} = I_{DC} + I_{Sig}. \tag{2}$$

Therefore, the emitted optical power $P_{Sig,TX}$ comprises a DC and an AC component, from which only the AC part is relevant. The here described optical system uses an OFDM waveform with frequency-selective bitloading for I_{Sig}. The reason for choosing an adaptive waveform is the simplicity to cope with frontend impairments due to the sophisticated driver, LED, PD and transimpedance amplifier setup maximizing bandwidth but yielding a frequency-selective SNR.

To determine the average optical power of the signal, the root mean square (RMS) modulation current is calculated. In comparison to sine signals, the peak-to-average power ratio (PAPR) or the so-called crest-factor C of the OFDM signal is used to derive the RMS current. Knowing the peak current $\hat{I}_{Sig,TX}$ of the transmitted signal, the RMS current $\bar{I}_{Sig,TX}$ can be calculated as

$$\bar{I}_{Sig,TX} = \hat{I}_{Sig,TX}/\sqrt{C}. \tag{3}$$

The optical output power of the signal can be calculated with

$$\bar{P}_{Sig,TX} = \bar{I}_{Sig,TX} \cdot \eta_{LED}, \tag{4}$$

whereby η_{LED} is the LED efficiency to convert electrical current into optical output power. Due to the limited aperture diameter of the transmitting lens and the full-width half-maximum (FWHM) divergence angle of the LED α, which is used for the determination of the transmitter lens diameter, a geometrical loss at the transmitter lens occurs. This loss is given as the ratio of the lens diameter $d_{lens,TX}$ and the enlarged optical spot in the distance of the focal length of the lens $d_{spot,f}$:

$$\gamma_{FWHM} = d_{lens,TX}/d_{spot,f}. \tag{5}$$

Note that distance between the LED and the transmitter lens is assumed equal to the focal length of the lens to achieve lowest divergence. Using lenses at the transmitter and receiver side adds reflection and absorption losses included in γ_{lens}.

$$\gamma_{lens} = \gamma_{lens,TX} + \gamma_{lens,RX}. \tag{6}$$

Coated lenses would further reduce these losses, but also increase cost.

For optical transmission, the atmospheric losses induced by reduced visibility are dominant. There are mainly three different models to predict the atmospheric loss based on visibility: the Al-Naboulsi model [33], the Kruse model [34] and the Kim model [35]. In the Al-Naboulsi model, advection and radiation fog are distinguished. Advection fog results from wet air, which cools down above the sea surface. Radiation fog is caused by cooling landmasses leading to a decrease of temperature of the overlying air layer. Because of different drop sizes, Al-Naboulsi characterizes the model for advection fog as

$$\beta_{N,adv}(\lambda) = (0.11478 \cdot \lambda + 3.8367)/V, \tag{7}$$

and the model for radiation fog as

$$\beta_{N,rad}(\lambda) = \left(0.18126 \cdot \lambda^2 + 0.13709 \cdot \lambda + 3.7502\right)/V, \tag{8}$$

whereby λ and V are the wavelength and visibility in kilometer, respectively. For advection and radiation fog attenuation can be calculated as

$$\gamma_{atm}^{N} = 10/\ln(10) \cdot \beta(\lambda). \tag{9}$$

The Kim and Kruse models calculate the attenuation described by the Beer-Lambert Law [36], [37] as follows

$$\gamma_{atm}^{KK} = 10\log\left(e^{-\sigma L}\right), \tag{10}$$

where L is the transmission distance. With [34] the scattering coefficient σ is

$$\sigma = \frac{3.91}{V}\left(\frac{\lambda}{550\,\text{nm}}\right)^{-q}, \tag{11}$$

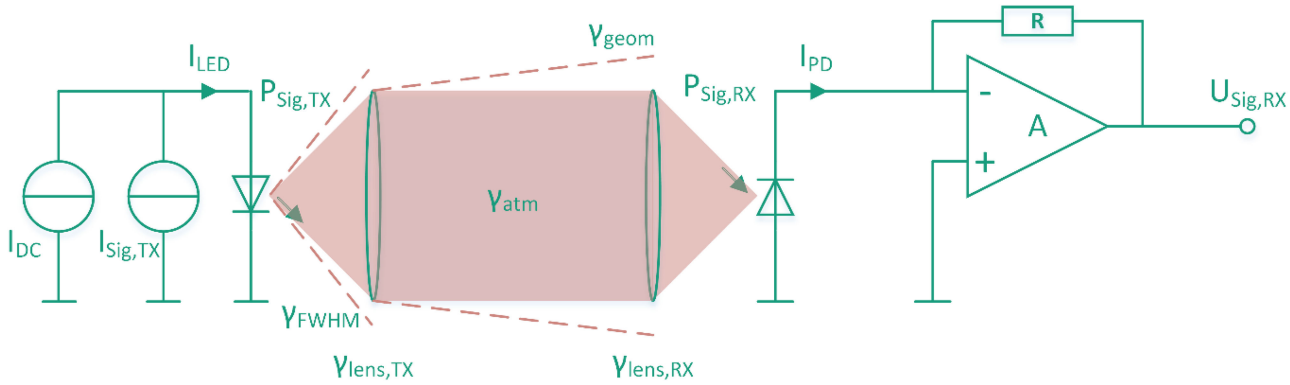

Fig. 2. Block diagram of the OWC system that is used for the outdoor measurements. The signal generation at the transmitter, the transmission in the atmosphere and reception are depicted for an unidirectional transmission.

with q being the empirical determined coefficient that indicates the size distribution of scattering. According to the Kruse model, the q parameter is

$$q = \begin{cases} 1.6, & V > 50\,\text{km}; \\ 1.3, & 6\,\text{km} < V < 50\,\text{km}; \\ 0.585 \cdot V^{\frac{1}{3}}, & V < 6\,\text{km}. \end{cases} \tag{12}$$

For the Kim model, the coefficient q is defined as

$$q = \begin{cases} 1.6, & V > 50\ \text{km}; \\ 1.3, & 6\,\text{km} < V < 50\,\text{km}; \\ 0.16 \cdot V + 1.34, & 1\,\text{km} < V < 6\,\text{km}; \\ V - 0.5, & 0.5\,\text{km} < V < 1\,\text{km}; \\ 0, & V < 0.5\,\text{km}. \end{cases} \tag{13}$$

In comparison to the Kruse model, the Kim model provides no wavelength dependency for low visibilities < 0.5 km. In this paper, the Kim model is used to calculate the atmospheric losses, because of the detailed definition of q for visibilities below 6 km and the comparison with measurement results, where a distinction between different fog types is not made. If the LOS is given, the constant geometrical loss represents the main weather-independent loss. Since, transmission distances between 50 and 250 m are considered in this paper, the influence of scintillation can be neglected [38], [39]. The constant geometrical loss

$$\gamma_{geom} = 10 \log \left(\frac{d_{lens,RX}}{d_{lens,TX} + 2 \cdot L \cdot \tan\Theta/2} \right)^2, \tag{14}$$

with

$$\Theta/2 = \arctan\left(d_{LED}/2 \cdot f_{lens,TX}\right), \tag{15}$$

depends on the diameter of both the transmitting and receiving aperture, denoted as $d_{lens,TX}$ and $d_{lens,RX}$, respectively, as well as the divergence half angle of the transmitter $\Theta/2$. At the transmission distance L, the divergence angle is calculated with the diameter of the LED emitting area d_{LED} and the focal length of the transmitter lens $f_{lens,TX}$, leading to an enlarged spot. Because of the small LED emitting area, the emitting beam diameter is approximated to zero. After considering all losses, the received optical power can be calculated as

$$\bar{P}_{Sig,RX} = \bar{P}_{Sig,TX} - \gamma_{FWHM} - \gamma_{lens} - \gamma_{atm} - \gamma_{geom}. \tag{16}$$

With the PDs photosensitivity ρ, the received optical power $\bar{P}_{Sig,RX}$ can be related to the RMS photocurrent $\bar{I}_{PD}$:

$$\bar{I}_{PD} = \bar{P}_{Sig,RX} \cdot \rho. \tag{17}$$

The transimpedance amplifier A, converts the photocurrent to the signal voltage $\bar{U}_{Sig,RX}$ as follows

$$\bar{U}_{Sig,RX} = \bar{I}_{PD} \cdot \delta, \tag{18}$$

where δ is the transimpedance of the amplifier. Here it is equal to the value of the feedback resistor R. The received signal's SNR can be calculated as

$$SNR_{Sig,RX} = \bar{U}_{Sig,RX}/\bar{U}_{noise}, \tag{19}$$

whereby $\bar{U}_{noise}$ is the total RMS noise voltage at the receiver, comprising shot and thermal noise of the PD and the following amplifier. When noise induced by background radiation can be eliminated by a small FOV, noise of an OW receiver is mainly determined by the voltage noise of the used transimpedance amplifier. For the sake of brevity, the complete derivation, including all noise sources is omitted and therefore the total noise voltage $\bar{U}_{noise}$ is given. Being able to calculate the received signal voltage and with the given total noise, the SNR for the here described system can be calculated. At first, the reference SNR is determined for different transmission distances by assuming 20 km visibility, i.e., practically no atm. attenuation. In Table 1, the values of the relevant parameters for the calculation are listed.

The loss induced by the limited size of the transmitter lens γ_{FWHM} is calculated using the LED half angle α and the focal length of the transmitter lens, resulting in a spot diameter of almost 100 mm in diameter at the lens. Since, the lens diameter is exactly 100 mm, half of the optical power is reaching the lens, leading to a 3 dB γ_{FWHM} loss. The two lenses at transmitter and receiver side, with a transmittance T_{lens} of 0.84, add a loss of $\gamma_{lens} = 1.5$ dB. For an OFDM signal a PAPR of 10 dB is assumed [40]. With the given values and the LED efficiency, the received power is calculated. With the photosensitivity ρ and

TABLE I
SYSTEM PARAMETERS FOR SNR AND DATA RATE PREDICTION

Parameter	Symbol	Value
LED DC current	I_{DC}	100 mA
Signal peak current	$\hat{I}_{Sig,TX}$	100 mA
LED efficiency	η_{LED}	0.25 W/A
Divergence half angle	α	17°
Lens aperture	$d_{lens,TX} = d_{lens,RX}$	100 mm
Focal length	$f_{lens,TX} = f_{lens,RX}$	166 mm
Transmittance	T_{lens}	0.84
Photosensitivity	ρ	0.55 A/W
Feedback resistor	R	3000 Ω
Total noise	$\overline{U}_{noise}$	304 nV / √Hz
Transmission distance	L	50 - 250 m
Visibility	V	20 km

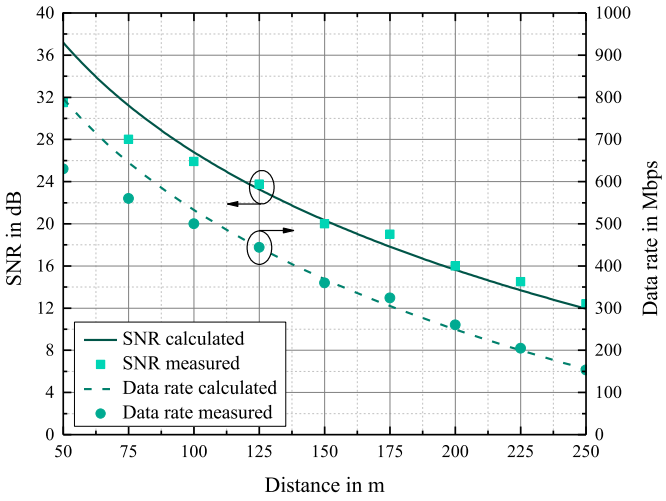

Fig. 3. Calculated SNR in dB (solid curve) and data rate in Mbps (dashed curve) for the OW system with the given parameters. The real measured SNRs and data rates are displayed as square and circle shapes. Atmospheric attenuation is zero to determine the link performance in ideal conditions.

the transimpedance of the amplifier A, related to the feedback resistor $R = 3$ kΩ, the photocurrent and the signal voltage are computed. With the given RMS noise voltage $\bar{U}_{noise}$, the SNR is calculated.

In Fig. 3, the SNR (solid curve) and the data rate (dashed curve) over distance are shown for the parameters from Tab. 1. In addition, SNR (square shape) and data rate (circle shape) values from field measurements are displayed. For distance ≥ 100 m, the model fits the measured values. For distances < 100 m, the model performs better than the real system. This can be attributed to nonlinearities from the non-ideal receiver, e.g., due to saturation effects, are not considered in the here presented model but may create distortions for higher input signals reducing the SNR.

In the following, the time variant atmospheric loss is used to predict the performance for the OWC system. External weather data freely available from airports worldwide enable the calculation of statistics for the visibility and attenuation, accordingly. Knowing climatic conditions and the properties of the transmission system, predictions of availability and capacity are possible, making the planning of a real deployment feasible in the first place. In Fig. 4(a), the cumulative distribution function (CDF)

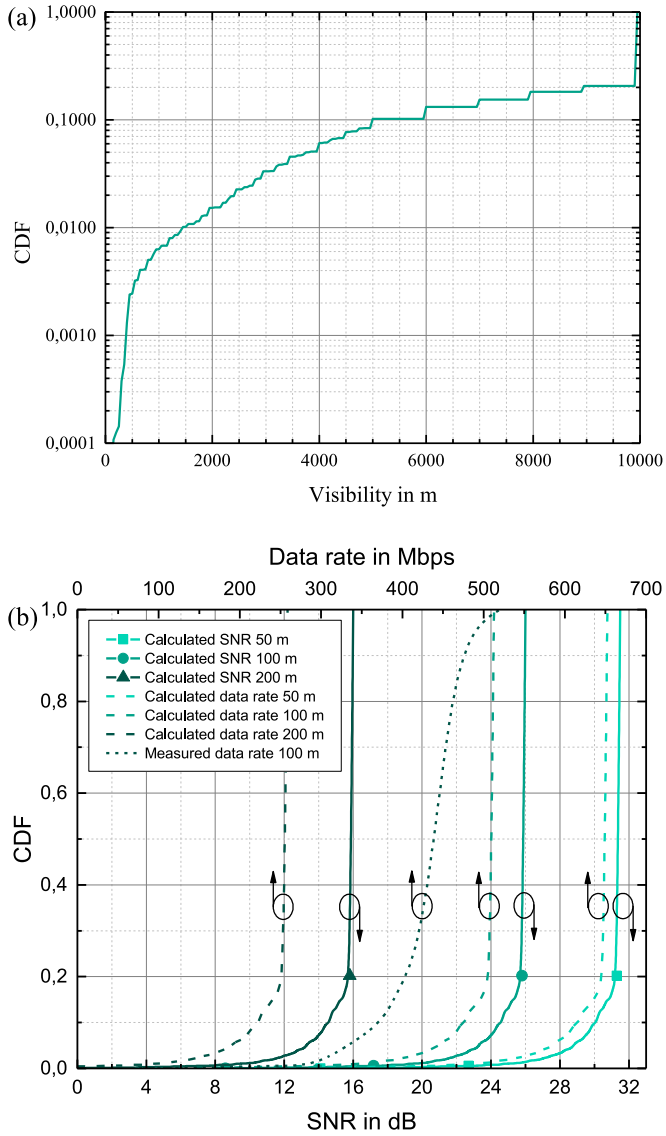

Fig. 4. (a) Cumulative distribution function for the external visibility values from Berlin Airport TXL, indicating high visibilities most of the time. (b) Predicted SNRs (solid curves) and data rates (dashed curves) for 50 m (light green curve), 100 m (green curve) and 200 m (dark green curve). Measured data rates at 100 m distance are displayed by the dotted curve. Distortions mentioned above, lead to a better prediction of 50 to 100 Mbps in comparison to the measurements.

for the visibility Berlin airport (TXL) is shown. The visibility is logged every 30 minutes with a maximum visibility of 10 km. To increase the number of samples and because of the large time granularity of the values, a period from 2011 to 2018 is chosen. With (11), the visibility CDF translates into an atmospheric loss distribution, introducing a statistic of atmospheric attenuation in the channel and thereby enabling the prediction of minimum data rates and availability for the given OWC system. With the calculated SNRs (solid curves) and data rates (dashed curves) from Fig. 4(b), the prediction leads to the CDFs for 50 m (light green curve), 100 m (green curve) and 200 m (dark green curve) transmission distance shown in Fig. 4(b). For 200 m link distance, the minimum data rate decreases to zero representing a link interruption. With Berlin's climatic conditions, the

maximum link distance for interruption free communication is obviously below 200 m for the given OWC setup. The dotted curve indicates the CDF values from the long-term measurement, described in detail in section III, representing the data rate for 100 m link distance. It can be observed that prediction is better than the measured data rates between 50 and 100 Mbps. The aforementioned nonlinear influences, cause differences to the visibility-based prediction. Nevertheless, the link has a higher SNR margin and hence is more robust for shorter transmission distances than needed for WTTH.

Similar predictions are performed for Tokyo (Japan) airport and Porto (Portugal) airport as well. An availability larger than 99.99% for a 100 m link transmission and minimum data rates of 62 Mbps and 458 Mbps are predicted for Tokyo and Porto airport, respectively. At Porto airport, lower atmospheric attenuation is present, which corresponds to higher available data rates.

III. Measurement Setup

Next to the data rate, the latency and availability are key parameters for 5G mobile FH and BH technologies as mentioned in Section I. In order to measure latency for different packet sizes and traffic loads as well as statistical results on the available data rates in an outdoor deployment, two measurement series were conducted with the OWC link. For the latency measurements, the protocol tester IXIA optixia XM2 with 1G Ethernet interfaces is used to generate traffic and to analyze the end-to-end latency of the packets being transmitted over the optical link.

For the OWC link, real-time transmission is achieved using a commercially available digital signal processing (DSP) chipset with 100 MHz bandwidth. Using an OFDM-like waveform and 12 bit/s/Hz spectral efficiency, allows for data rates up to 1 Gbps. Data is supplied via a standard Ethernet interface. All physical and medium access layer functionalities as well as digital to analog and analog to digital conversion are performed by the chipset. The converted digital input signal is analogously forwarded to the optical frontend (OFE), including an LED driver for bandwidth enhancement and a high-sensitive photoreceiver with a large area Si-PIN PD. Please note that both parts of the OFE provide bandwidths of 200 MHz and a flat system frequency response is achieved. The latency measurements are conducted in static laboratory conditions. Since, outdoor channel conditions are changing rather slowly in the range of seconds, the results are also valid for real outdoor applications. For the used DSP chip, latency peaks are only expected for rapid changes [41]; hence constant low latencies are presumed for the described application.

To obtain results on availability and to compare the OWC link to mm-wave technology, a DSP in combination with an OFE was setup in a waterproof housing outdoors. The infrared LED (OSRAM) SFH 4451 with a wavelength of 850 nm has an active area of 0.3 mm $\times$ 0.3 mm, which is enlarged to 1.8 mm^2 by a parabolic concentrator to achieve a FWHM angle of 17°. For the photoreceiver the large area Si-PIN PD Hamamatsu S6968 is used. The large area allows for alignment tolerances and gains robustness for vibrations, e.g., caused by wind, while the photoreceiver enables high bandwidths. As discussed above, geometrical loss needs to be reduced, which is achieved using a convex lens at the transmitter with 100 mm diameter and 166 mm focal length reducing divergence. Please note that 166 mm is the exact focal length needed to match the 17°FWHM angle of the LED. To reduce the geometrical loss further, the same convex lens is used at the receiver, leading to an enlarged effective active area of the PD, whereby the geometrical loss from more than 70 dB with no lenses is reduced to 20 dB at 100 m. In addition, the field-of-view (FOV) is reduced. Increasing the receiving lens radius to 200 mm and the focal length of the transmitting lens to 300 mm would reduce the geometrical loss significantly to 3.5 dB at 100 m, however, the system form factor would be substantially increased. Please note that the OWC system offers no link margin. Time variant atmospheric losses have direct influence on the data rate but in good weather conditions, the bandwidth is used in the most efficient way, leading to high data rates. For the mm-wave link, Siklus commercial single carrier 60 GHz EtherHaul 600 in the license free V-band, with 500 MHz signal bandwidth and coarse rate adaptation up to 64 quadrature amplitude modulation (QAM) is installed. The EtherHaul 600 enables the choice of carrier frequency from 57 to 64 GHz, enabling interference avoidance with mm-wave systems nearby. An integrated 35 dBi antenna allows for robust communication in challenging atmospheric conditions. Similar to the OWC system, data can be applied by an Ethernet interface. More information can be found in [42]. Both links are installed on the rooftop of the Fraunhofer Heinrich Hertz Institute (HHI) building in Berlin, Germany and on the rooftop of the Technische Universität Berlin (TUB), Germany. Thereby a transmission distance of 100 m was achieved, with a height difference of 25 m, simulating a MC to SC scenario. To enable the analysis of the influences from various weather conditions on both link performances, a weather sensor Vaisala PWD22 was installed. Precipitation, i.e., rain or snow, as well as the visibility up to 20 km are logged every 30 s. Fig. 5(a) shows photographs of the outdoor measurement site and Fig. 5(b) the two installed links on the HHI rooftop.

IV. Measurement Results

During the measurement period, various atmospheric conditions were observed with low visibilities and resulting atmospheric losses up to 240 dB/km. Since, a different behavior for the OWC and the mm-wave link is expected, a correlation analysis between both links is performed. In Fig. 6(a), the SNR values for the optical link are plotted against the values for the mm-wave link. Each cross indicates an OWC SNR and corresponding mm-wave SNR value, which was measured at the same time and therefore with the same weather condition. It can be observed, that the OWC SNR and mm-wave SNR varies from 3 dB to 27 dB and 11 dB to 19 dB, respectively. Moreover, the area in the bottom left corner of the correlation plot without dots indicate that for bad weather situations, at least one link provides good performance. The different carrier frequencies lead to mainly different performance for the same weather situation. OWC SNR and mm-wave SNRs are reduced at different times,

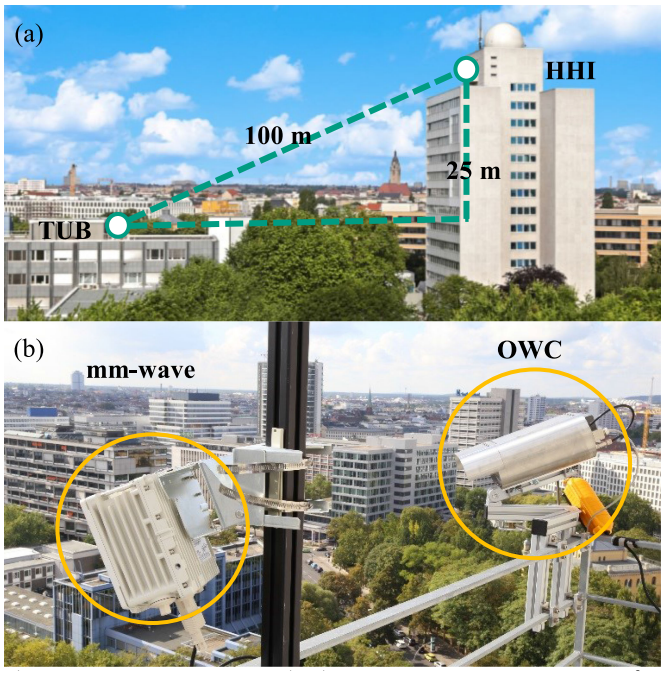

Fig. 5. (a) OWC and mm-wave link in an outdoor deployment on the rooftop of the HHI and the TUB. A transmission distance of 100 m with a height difference of 25 m is realized. (b) OWC link in outdoor housing and mm-wave link installed in parallel.

resulting in a weak correlation. A hybrid link approach would therefore have increased robustness and data rate. This effect is observed exemplarily in the measurements from January 10 and 11 2018, shown in Fig. 6(b)–(e). A bad weather event occurred on January 10 at 6 am, resulting in a visibility drop from 16000 m down to 100 m, depicted in Fig. 6(b). The atmospheric attenuation is, calculated with the Kim model and visualized in Fig. 6(d). The OWC link's SNR is depicted in Fig. 6(e) (light green curve); the data rate reduces to 60 Mbps. Despite the high atmospheric attenuation of up to 170 dB/km, the link was not interrupted. Please note that the reduced visibility effect on the mm-wave SNR is almost negligible, shown in Fig. 6(e) (dark green curve). On January 11 at 8 am a rain event starts, which is depicted in Fig. 6(c). This caused an opposite effect with a reduction of the mm-wave SNR while the optical SNR remains constant. During the complete measurement period, the impairments on the OWC link due to low visibility were higher than the rain induced effects on the mm-wave link. Nevertheless, the visibility statistic shows mostly good weather conditions with visibilities $>$ 1000 m in 99.2% of the time. As a result, the rate adaptive approach is validated. The bandwidth is used efficiently and no static link margin is wasted. Furthermore, a statistical evaluation of the SNRs yields to the cumulative distribution function in Fig. 6(f). Here it can be seen that the optical link's overall performance is good, despite single bad weather events with higher atmospheric attenuations and larger variations of the SNR compared to the mm-wave link. 99.8% of all measured data rates were higher for the optical link, while the mm-wave link is more consistent. Visibilities larger than the transmission distance have only low influence on the optical link and rate

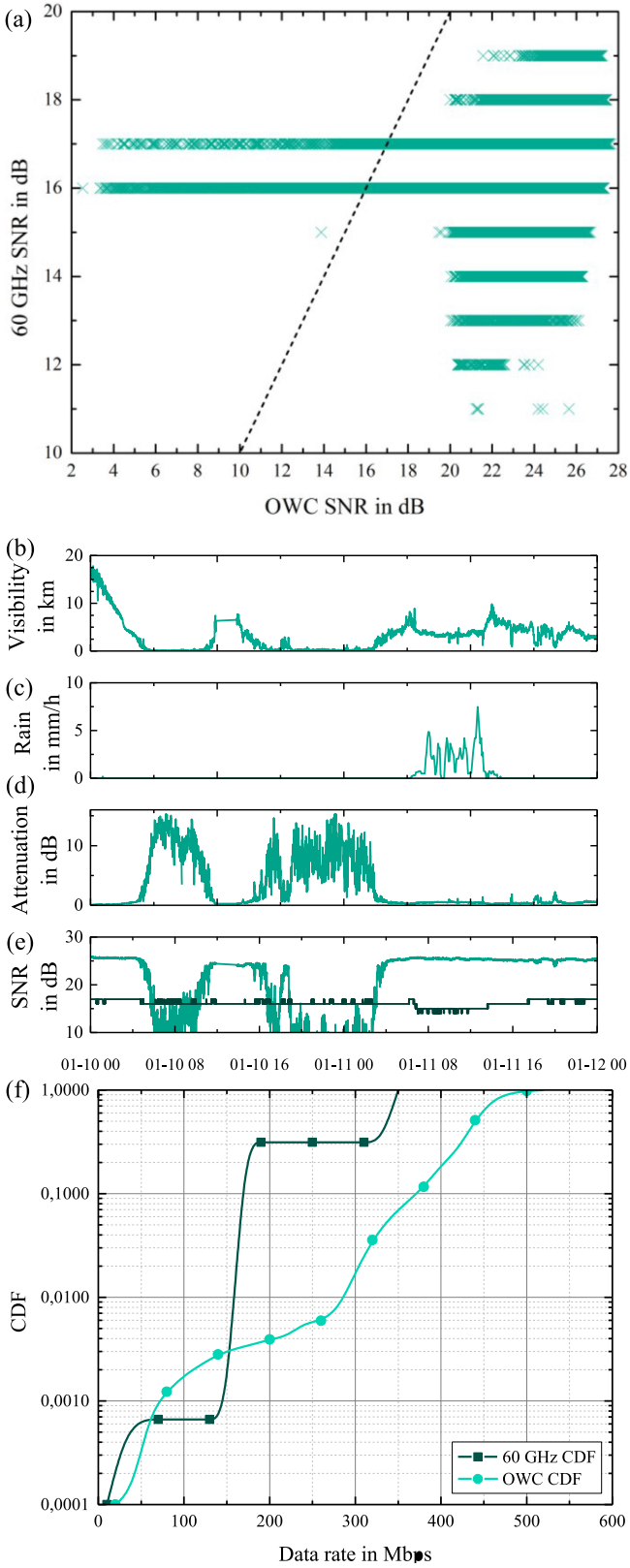

Fig. 6. (a) 60 GHz SNR values plotted versus the corresponding OWC SNR values, yielding a weak correlation between both link technologies The dotted line represents a strong correlation of 1. (b)–(e) Exemplary weather event on January 10 and 11, with a low visibility event and rain shown in (b) and (c), resulting in 170 dB/km atmospheric attenuation shown in (d). The OWC and 60 GHz SNR shown in (e) are reduced according to the loss but not interrupted. (f) CDF for the OWC link and the mm-wave link.

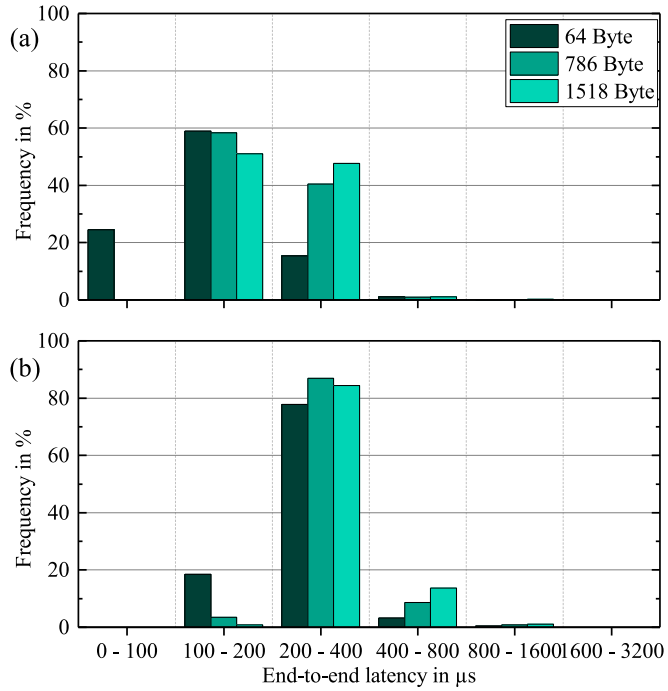

Fig. 7. Relative frequency of the latency for (a) 100 Mbps traffic load, and (b) 500 Mbps traffic load.

adaptation provides additional robustness for rarely occurring high atmospheric losses. Both links offered more than 99.99% availability during the complete measurement period.

Next to the data rates, the latency was measured under several load conditions. In Fig. 7(a), the end-to-end latency for 100 Mbps and Fig. 7(b) 500 Mbps throughput is shown with respect to different frame sizes. All packets have latencies below 1600 μs, more than 99% below 800 μs and 90% between 100 and 400 μs.

The performed long-term data rate and latency measurements show that the OWC data rates are comparable and even outperform the mm-wave link most of the time with latencies below 1 ms even for high traffic loads. Thereby, OWC offers a low-cost alternative, matching the requirements for BH of SCs and WTTH. Since the OFE bandwidths for both the transmitter and the receiver are 200 MHz, the potential for even higher data rates is given. Additional measurements in laboratory conditions were conducted with a new generation of the DSP chipset, offering 200 MHz bandwidth and peak rates of up to 2 Gbps. Thereby the requirements for lower SPs or more demanding WTTH specifications can be served in future setups.

V. Conclusions

In this paper, we presented a mathematical model for an OW link and the prediction of the link performance for different transmission distances was compared with real field measurements. The model shows reasonable agreement between theory and measurement, based on the measured visibility. By using freely available external weather data from airports, the prediction of the link performance is possible for any climatic condition; hence enabling the planning of a real deployment. In addition, results from an ongoing long-term measurement, using an OWC link, showed the suitability for the BH of small radio cells and WTTH. Statistical visibility data validate the mostly good conditions for the OWC link transmission, resulting in high probabilities for high data rates. A correlation analysis for the OWC and the mm-wave link showed weak correlation; therefore, a hybrid link approach will have both higher robustness and data rate. The link performance was analyzed for exemplary weather events, which confirmed the robustness of the rate adaptive link setup. Both links were not interrupted during the whole measurement period, corresponding to an availability higher than 99.99%. The statistical analysis conducted over the entire measurement indicates that the OWC link data rates are comparable and even outperform the mm-wave link most of the time. A latency measurement with high traffic load showed latencies for all and for 99% of the packets below 1600 μs and below 800 μs latency, respectively. Laboratory measurements with a new DSP chip generation indicated the potential for higher data rates, by exploiting the full bandwidth of the current OFE.

Data rates, latencies and availability of the OWC link satisfy the needs for the BH of small cells, even for diverse SPs, and for WTTH as a wireless last mile solution. Laser based concepts offer multiple GHz bandwidth to increase data rates manifold for future 5G applications.

References

[1] NGMN Alliance, "NGMN 5G white paper," Frankfurt, Germany, White Paper, 2015.
[2] 5GPPP, "5G key performance indicators." 2014. [Online]. Available: https://5g-ppp.eu/kpis/, Accessed on: Jun. 20, 2018.
[3] M. Jaber, M. A. Imran, R. Tafazolli, and A. Tukmanov, "5G backhaul challenges and emerging research directions: A survey," *IEEE Access*, vol. 4, pp. 1743–1766, 2016.
[4] Z. Roth *et al.*, "Vision and architecture supporting wireless GBit/sec/km^2 capacity density deployments," in *Proc. Future Netw. Mobile Summit*, pp. 1–7, 2010.
[5] V. Jungnickel *et al.*, "The role of small cells, coordinated multipoint, and massive MIMO in 5G," *IEEE Commun. Mag.*, vol. 52, no. 5, pp. 44–51, May 2014.
[6] S. Tombaz, P. Monti, F. Farias, M. Fiorani, L. Wosinska, and J. Zander, "Is backhaul becoming a bottleneck for green wireless access networks?," in *Proc. IEEE Int. Conf. Commun.*, 2014, pp. 4029–4035.
[7] Huawei Press, "Huawei launches first urban 5G 'wireless to the home' CPE trial in North America," Huawei Press, Shenzhen, China, 2018. [Online]. Available: https://www.huawei.com/en/press-events/news/2018/2/first-urban-5G-Wireless-Home-CPE-trial. Accessed on: Jul. 16, 2018.
[8] Deutsche Telekom, "A new way to build and deploy telecom infrastructure," Deutsche Telekom, Bonn, Germany. [Online]. Available: https://www.telekom.com/en/blog/group/article/a-new-way-to-build-and-deploy-telecom-infrastructure-507960. Accessed on: Jul. 18, 2018.
[9] U. Dötsch, M. Doll, H.-P. Mayer, F. Schaich, J. Segel, and P. Sehier, "Quantitative analysis of split base station processing and determination of advantageous architectures for LTE," *Bell Labs Tech. J.*, vol. 18, no. 4, pp. 105–128, 2014.
[10] China Mobile, "C-RAN: The road towards green RAN," Beijing, China, White Paper Version 2.5, pp. 15–16, 2011.
[11] Ericsson AB, Huawei Technologies Co. Ltd, NEC Corporation, Alcatel Lucent, and Nokia Networks, "CPRI Specification V7.0 (2015-10-09)," Common Public Radio Interface Specification, 2015.
[12] D. Harutyunyan, R. Riggio, and F. B. K. Create-net, "Flexible functional split in 5G networks," *IEEE Trans. Netw. Serv. Manage.*, vol. 15, no. 3, pp. 961–975, Sep. 2017.

[13] A. Aijaz, H. Aghvami, and M. Amani, "A survey on mobile data offloading: Technical and business perspectives," *IEEE Wireless Commun.*, vol. 20, no. 2, pp. 104–112, Apr. 2013.
[14] H. Ishii, Y. Kishiyama, and H. Takahashi, "A novel architecture for LTE-B:C-plane/U-plane split and phantom cell concept," in *Proc. IEEE Globecom Workshops*, 2012, pp. 624–630.
[15] D. Wübben *et al.*, "Benefits and impact of cloud computing on 5G signal processing: Flexible centralization through cloud-RAN," *IEEE Signal Process. Mag.*, vol. 31, no. 6, pp. 35–44, Nov. 2014.
[16] L. Grobe *et al.*, "High-speed visible light communication systems," *IEEE Commun. Mag.*, vol. 51, no. 12, pp. 60–66, Dec. 2013.
[17] S. Shao *et al.*, "Design of a visible-light-communication enhanced WiFi system," *IEEE/OSA J. Opt. Commun. Netw.*, vol. 7, no. 10, pp. 960–973, Oct. 2015.
[18] P. W. Berenguer *et al.*, "Optical wireless MIMO experiments in an industrial environment," *IEEE J. Sel. Areas Commun.*, vol. 36, no. 1, pp. 185–193, Jan. 2018.
[19] C. Lee *et al.*, "Gigabit-per-second white light-based visible light communication using near-ultraviolet laser diode and red-, green-, and blue-emitting phosphors," *Opt. Express*, vol. 25, no. 15, pp. 17 480–17 487, 2017.
[20] Y. Wang, X. Huang, L. Tao, and N. Chi, "1.8 Gb/s WDM VLC over 50-meter outdoor free space transmission employing CAP modulation and receiver diversity technology," in *Proc. Opt. Fiber Commun. Conf. Exhib.*, 2015, pp. 7–9.
[21] Y. Wang, X. Huang, J. Shi, Y. Wang, and N. Chi, "Long-range high-speed visible light communication system over 100-m outdoor transmission utilizing receiver diversity technology," *Opt. Eng.*, vol. 55, no. 5, 2016, Art. no. 056104.
[22] J. Yoo, J. Jang, J. Kwon, H. Kim, D. Song, and S.- Jung, "Demonstration of vehicular visible light communication based on LED headlamp," *Int. J. Automot. Technol.*, vol. 17, no. 2, pp. 347–352, 2016.
[23] H. Kaushal, G. Kaddoum, V. K. K. Jain, and S. Kar, "Experimental investigation of optimum beam size for FSO uplink," *Opt. Commun.*, vol. 400, pp. 106–114, 2017.
[24] H. Kaushal and G. Kaddoum, "Applications of lasers for tactical military operations," *IEEE Access*, vol. 5, pp. 20736–20753, 2017.
[25] H. Kaushal and G. Kaddoum, "Free space optical communication: Challenges and mitigation techniques," *IEEE Commun. Surveys Tuts.*, vol. 19, no. 1, pp. 57–96, 2015.
[26] "Ronja by Twibright Labs," 2006. [Online]. Available: http://ronja.twibright.com/. Accessed on: Jul. 13, 2018.
[27] "Koruza–Light-speed networking," [Online]. Available: http://www.koruza.net/. Accessed on: Jul. 13, 2018.
[28] D. Schulz *et al.*, "Long-term outdoor measurements using a rate-adaptive hybrid optical wireless/60 GHz link over 100 m," in *Proc. Int. Conf. Transparent Opt. Netw.*, 2017, pp. 1–4.
[29] D. Schulz, J. Hohmann, J. Hilt, P. Hellwig, R. Freund, and V. Jungnickel, "Measurement based correlation analysis of a hybrid optical wireless/60 GHz link," in *Proc. Global LIFI Congr.*, 2018, pp. 1–4.
[30] D. Schulz *et al.*, "Optical wireless LED link for the backhaul of small cells," in *Proc. Opt. Fiber Commun. Conf. Exhib.*, 2015, pp. 1–3.
[31] 3GPP, "Study on channel model for frequencies from 0.5 to 100 GHz (Release 15)," 3GPP, Sophia Antipolis, France, Tech. Rep. TR 38.901, Jun. 2018.
[32] L. Thiele, M. Peter, and V. Jungnickel, "Statistics of the Ricean k-factor at 5.2 GHz in an urban macro-cell scenario," in *Proc. IEEE 17th Int. Symp. Pers. Indoor Mob. Radio Commun.*, 2006, pp. 1–5.
[33] M. A. Naboulsi and F. de Fornel, "Fog attenuation prediction for optical and infrared waves," *Opt. Eng.*, vol. 43, no. 2, pp. 319–329, 2004.
[34] P. W. Kruse, L. D. McGlauchlin, and R. B. McQuistan, *Elements of Infrared Technology: Generation, Transmission, and Detection*. New York, NY, USA: Wiley, 1962.
[35] I. I. Kim, B. McArthur, and E. J. Korevaar, "Comparison of laser beam propagation at 785 nm and 1550 nm in fog and haze for optical wireless communications," *Proc. SPIE*, vol. 4214, pp. 26–37, 2001.
[36] P. Bouguer, *Essai d'optique, Sur la gradation de la lumière*, Bibliothèque nationale de France, Paris, 1729.
[37] A. Beer, "Bestimmung der Absorption des rothen Lichts in farbigen Flüssigkeiten," *Ann. Der Phys. Und Chemie*, vol. 86, pp. 78–88, 1852.
[38] A. Prokes, "Modeling of atmospheric turbulence effect on terrestrial FSO link," *Radioengineering*, vol. 18, no. 1, pp. 42–47, 2009.
[39] I. I. Kim, "Measurement of scintillation for free-space laser communication at 785 nm and 1550 nm," *Proc. SPIE*, vol. 3850, pp. 49–62, 1999.
[40] T. Jiang and Y. Wu, "An overview: Peak-to-average power ratio reduction techniques for OFDM signals," *IEEE Trans. Broadcast.*, vol. 54, no. 2, pp. 257–268, Jun. 2008.
[41] P. W. Berenguer *et al.*, "Real-time optical wireless communication: Field-trial in an industrial production environment," in *Proc. ECOC*, 2018, pp. 1–3.
[42] Siklu, "EtherHaul hundred series," Siklu, Fort Lee, NJ, USA, 2018. [Online]. Available: https://www.siklu.com/product/etherhaul-hundred-series/. Accessed on: Oct. 9, 2018.

Dominic Schulz received the M.Eng. degree in communications engineering from Berlin University of Applied Sciences, Berlin, Germany, in 2012, and is currently working toward the Ph.D. degree in the field of optical wireless communications. After the Master's degree, he joined the Department of Photonic Networks and Systems, Fraunhofer Institute for Telecommunications, Heinrich Hertz Institute. His current activities include the development of high data rate systems for wireless access, as well as research toward long-range links.

Julian Hohmann received the M.Eng. degree in communications engineering from Berlin University of Applied Sciences, Berlin, Germany, in 2017. In 2017, he was with the Department of Photonic Networks and Systems, Fraunhofer Institute for Telecommunications, Heinrich Hertz Institute. His current activities are in the areas of optical wireless communication, including the development of systems for outdoor point-to-point applications.

Peter Hellwig received the Diploma degree in electrical engineering from Berlin University of Applied Sciences, Berlin, Germany, in 2009. In 2016, he joined the Fraunhofer Institute for Telecommunications, Heinrich Hertz Institute, Berlin, Germany, where he is currently an Electrical Engineer with the Department of Photonic Networks and Systems. His current activities include the areas of design and realization of visible light communication systems.

Jonas Hilt received the Diploma degree in electrical engineering from Berlin University of Applied Sciences, Berlin, Germany, in 2009. In 2009, he joined the Fraunhofer Institute for Telecommunications, Heinrich Hertz Institute, Berlin, Germany, where he is currently an Electrical Engineer with the Department of Photonic Networks and Systems. His current activities include the areas of design and realization of embedded systems and visible light communication systems.

Christian Schmidt (GS'12) received the B.Sc. degree from Kiel University, Kiel, Germany, in 2012, and the M.Sc. degree from the Karlsruhe Institute of Technology, Karlsruhe, Germany, in 2014. Since 2015, he has been with the Fraunhofer Institute for Telecommunications, Heinrich-Hertz-Institute, Berlin, Germany. His current research interests include interleaving concepts for next generation high-speed digital-to-analog converters.

Ronald Freund received the Dipl.Ing. and Dr.Ing. degrees in electrical engineering from the Technical University of Ilmenau, Ilmenau, Germany, in 1993 and 2002, respectively, and the MBA degree from RWTH Aachen, Aachen, Germany, in 2013. Since 1995, he has been with the Heinrich Hertz Institute, Berlin, Germany, where he is currently leading the Department of Photonic Networks and Systems. Since 2017, he is a Professor in photonic communication systems with the Technical University Berlin, Berlin, Germany.

Volker Jungnickel (M'99) received the Doctorate degree in physics from Humboldt University Berlin, Berlin, Germany, in 1995, and the Habilitation degree in communications engineering from Technical University Berlin, Berlin, Germany, in 2015. In 1997, he joined Fraunhofer Heinrich Hertz Institute, Berlin, Germany, where he contributed to high-speed optical wireless communications, the first 1 Gb/s mobile radio link, the first real-time trials of LTE, and the first coordinated multipoint trials for LTE. He is currently leading the Metro-, Access, and In-house Systems group working on short-range optical technologies. He also serves as the Chair of the IEEE 802.15.13 task group on Multi-Gbit/s Optical Wireless Communications. Since 2002, he has been with the Technical University, Berlin, teaching courses on MIMO and adaptive transmission.